ICARUS 51, 391–415 (1982)

Temporal Variability of Ultraviolet Cloud Features in the Venus Stratosphere[1]

ANTHONY D. DEL GENIO[2] AND WILLIAM B. ROSSOW

NASA Goddard Space Flight Center, Institute for Space Studies, 2880 Broadway, New York, N.Y. 10025

Received November 13, 1981; revised March 2, 1982

Statistics on the temporal variability of uv cloud features on Venus during 66 days of nominal mission imaging by the Pioneer Venus Orbiter Cloud Photopolarimeter reveal at least five types of systematic variability on large scales: (1) a low-latitude global-scale wave of period 3.94 ± 0.1 days corresponding to longitudinal motion of the dark equatorial band and propagating westward relative to the mean flow; (2) a midlatitude wave of period 5.20 ± 0.2 days corresponding to wavenumber 1 oscillations of the latitude of the bright polar bands and propagating eastward relative to the mean flow; (3) ~2- to 3-week fluctuations in the slope of longitudinal cloud brightness power spectra at intermediate wavenumbers manifested by variations in the intensity of large bow-shaped features; (4) ~2-month variations in polar region brightness consistent with polar brightening episodes observed from Earth; and (5) a monotonic decrease in the disk-integrated brightness of Venus during the nominal mission which may be either a true time variation or a solar-locked longitudinal dependence of brightness. Small-scale features appear to correlate with large-scale albedo patterns. Specifically, cellular features exist primarily where large-scale dark material is present, while the orientation of streak features with respect to latitude circles oscillates with the same ~4-day period as the large-scale features at low latitudes. The wide range of time scales present in the data suggests the complexity of Venus stratospheric dynamics. Extended observations over many years may be necessary to define the general circulation.

I. INTRODUCTION

Definition of the general circulation of the upper cloud region of the Venus atmosphere (60–70 km) and elucidation of the dynamic and radiative processes which maintain it are two of the primary goals of the Pioneer Venus mission. The flow at these levels is dominated by a strong easterly zonal wind at all observed latitudes, some 50 times faster than the planetary rotation velocity (Counselman *et al.*, 1980; Rossow *et al.*, 1980). The angular momentum of this flow is small, though, compared to that of the circulation in the atmosphere below the clouds (cf. Fig. 7 in Schubert *et al.*, 1980). This suggests that a relatively inefficient mechanism transports a small fraction of the lower atmosphere angular momentum up to cloud levels to produce the observed winds. Of prime interest is the extent to which this vertical transport is accomplished by eddies stimulated by diurnal heating (cf. Young and Schubert, 1973; Fels and Lindzen, 1974) or by a mean meridional circulation driven by latitudinal variations of insolation (Gierasch, 1975). The latter mechanism also requires eddies in order to work, but these must be quasi-barotropic, transporting angular momentum primarily equatorward while exchanging negligible amounts of heat (Rossow and Williams, 1979).

Insight into the problem can be gained by studying the variability of the Venus atmosphere and searching for signatures of the relevant eddy processes. The images from the Pioneer Venus Orbiter Cloud Photopolarimeter (OCPP) experiment (Travis *et al.*, 1979a,b; Rossow *et al.*, 1980) provide cru-

[1] Paper presented at "An International Conference on the Venus Environment," Palo Alto, California, November 1–6, 1981.

[2] M/A-COM Sigma Data Inc., 2880 Broadway, New York, N.Y. 10025.

0019-1035/82/080391-25$02.00/0

cial information about variability in the form of cloud-tracked wind velocities and the changing morphology of ultraviolet cloud albedo patterns at 365-nm wavelength. The OCPP data complement previous observations of atmospheric fluctuations at upper cloud levels. For example, a comparison of Mariner 10 and preliminary OCPP observations has already demonstrated that the latitudinal profile of zonal wind can change significantly with time (Rossow *et al.*, 1980). Ground-based uv observations of short- and long-term evolution of the appearance of Venus (Dollfus, 1975) also suggest a time-dependent flow and invite comparisons with OCPP images. These observations imply that monitoring of Venus over long periods of time may be necessary to determine the "mean" state of the atmosphere. Furthermore, given the stochastic nature of atmospheric processes, even the shorter time scales of variation can be characterized only by good temporal statistics of fluctuations over a wide range of spatial scales. The Pioneer Venus mission provides us with a unique opportunity to assemble better global eddy statistics for this region of the atmosphere.

To understand the processes which maintain the strong zonal winds, we would ideally like to calculate eddy momentum transports, kinetic energy levels, and energy conversion rates over the globe. Eventually, some of this information may be retrievable from cloud-tracked winds, but thus far, only limited attempts have been made, using Mariner 10 data spanning only 3 days (Limaye and Suomi, 1981). The 10–20 m/sec uncertainties in individual velocity determinations require averaging to improve accuracy and limit results to only the largest-scale eddies on time scales on the order of 1 week or longer. To resolve a wider range of space and time scales, we employ an alternative approach utilizing the uv cloud brightness distribution itself. Unfortunately, the identity of the absorber(s) responsible for uv features at wavelengths longer than 320 nm is still unknown,[3] so a direct correspondence between uv contrasts and fluctuations in dynamic state variables (e.g., velocity, temperature) cannot yet be deduced.

The complexity of the Venus cloud system only exacerbates the problem of interpreting cloud features. Contrasts in the uv images are caused by at least three types of substances: (1) bright ~1-μm H_2SO_4 droplets which compose the main visible cloud; (2) the unknown uv absorber(s), which may be gaseous and/or particulate, embedded within the 1-μm aerosol layer; and (3) a brighter submicron haze which exists within and above the 1-μm cloud (Kawabata *et al.*, 1980, 1982; Lane and Opstbaum, 1982). Given the microphysical constraints on the lifetimes and relative motions of such particles, the wide range of observed space and time scales in the images is not easily explained (Rossow *et al.*, 1980). The haze has its greatest uv optical depth in the polar regions and probably accounts for much of what we see there. At lower latitudes the haze uv optical thickness is very small so that only the 1-μm droplets and uv absorber(s) are important in producing uv patterns. As a result, we may see to varying depths over the ~60- to 70-km altitude range at low latitudes, and generally a few kilometers higher nearer the poles due to increased haze and longer slant paths. Thus, care must be exercised in interpreting the image data, particularly when comparisons of different latitudes are involved.

Despite these uncertainties, cloud brightness spectra based on Mariner 10 and Pioneer Venus uv images of Venus (Travis, 1978; Rossow *et al.*, 1980), if interpreted to represent the eddy kinetic energy spectrum, appear to be consistent with expectations about the nature of large-scale turbulence in a slowly rotating stratosphere (Rossow and Williams, 1979). Travis (1978)

[3] SO_2 has been identified as the major uv absorber in the 200- to 320-nm wavelength range. However, it cannot by itself account for the contrast at 365 nm (Esposito, 1980).

has also calculated terrestrial cloud brightness spectra in the same manner and reproduced the major features of the terrestrial eddy kinetic energy spectrum. In fact, cloud brightness has often been used directly to reveal the propagation characteristics of tropical disturbances on Earth (cf. Chang, 1970; Zangvil, 1975). These results lend some confidence in applying similar procedures to Venus, but the microphysical processes responsible for the maintenance of the Venus clouds are very different from those characterizing terrestrial water clouds (Rossow, 1978), so the use of terrestrial clouds as tracers of eddy processes does not guarantee similar success on Venus. Nonetheless, the uv features must reflect the cloud level dynamics in some manner, and systematic description of the cloud brightness distribution and its variation may enable us to glimpse the nature of the eddies and their interaction with the mean flow.

In Section II we describe the properties of the OCPP image data set and the processing techniques used for quantitative analysis. We then examine short-term variations of uv cloud brightness (Section III) suggestive of propagating planetary-scale waves. Evidence of longer-term uv variability, i.e., on time scales in excess of one to two cloud-level rotation periods, is presented in Section IV. Possible implications of these findings for certain aspects of the stratospheric dynamics are discussed in Section V. We summarize our results in Section VI.

II. IMAGE CHARACTERISTICS AND PROCESSING

OCPP images are obtained during the high-altitude apoapsis portion of the highly inclined and eccentric 24-hr Pioneer Venus orbit by a spin-scan technique (Russell *et al.*, 1977; Travis *et al.*, 1979a; Travis, 1979). An average of ~4 hr is required to generate a full-disk image in this way. It is therefore possible to produce as many as four complete images per day, although no more than three were acquired on any nominal mission orbit due to the necessity for complementary polarimetry, limb-scan, and partial-disk imaging observations during the same period. In order to have a time record with regular sampling, we averaged all data used in quantitative temporal analyses over 1-day intervals.

Since the spacecraft orbit is fixed in an inertial reference frame, the phase angle (Sun–planet–observer) of disk center changes by 1.6°/day. The images used in this paper come from a 66-day period in 1979 (orbits 34–99) during which at least one full-disk image per day was acquired and the phase angle never exceeded 60°. Thus variations on time scales from several days up to 1–2 months can be examined. Unfortunately, there are reasons to suspect that the zonal circulation and eddy kinetic energy level may vary over time intervals as long or longer than this (Rossow *et al.*, 1980). Information on these longer time scales can be obtained reliably only by comparing results from many imaging periods.

Coverage of the southern hemisphere is generally somewhat better than that of the northern hemisphere due to the 17°N latitude of periapsis of the orbit. As a result, coverage poleward of ~55°N latitude is sporadic, while in the southern hemisphere good coverage always exists up to at least 70° latitude. The earliest images in the nominal mission sequence show the morning quadrant; they shift gradually to full phase (orbit 71) and thereafter show the afternoon quadrant at increasing phase angles. Therefore, long-term variations cannot be distinguished from large-scale longitudinal variations on the basis of nominal mission data alone.

Variations in scattering geometry over the disk and with time and position in the orbit produce apparent brightness variations in the raw data which do not reflect actual variations in cloud structure. These variations are removed by normalization, using a scattering model for the clouds. We

first navigate the image, utilizing information on the spacecraft's instantaneous position relative to Venus and the pointing direction of the OCPP telescope. The input cloud model is a vertically homogeneous deck of pure 1.05-μm H_2SO_4 droplets with optical properties as determined by Hansen and Hovenier (1974). Using this cloud model, we calculate the theoretical intensity for unit solar flux as a function of position on the visible disk for a horizontally uniform atmosphere whose spherical albedo matches that of Venus at $\lambda = 365$ nm. We use a current version of the fast invariant imbedding technique for multiply-scattering atmospheres based on the work of Sato *et al.* (1977). Next, a normalizing factor designed to be independent of scattering geometry is defined as the ratio of the disk-integrated (summing equally over all pixels) raw and theoretical intensities; this factor is, in effect, the intrinsic brightness of Venus as observed from a very large distance. Finally, the appropriate theoretical intensity (I^t) for each pixel is scaled by the normalizing factor (I^d) and subtracted from the raw brightness (I^r). Thus the normalized brightness (I^n) at each point is an estimate of the intrinsic cloud brightness deviation from the disk-integrated intensity:

$$I^n = I^r - I^d I^t = I^r - I^t \left(\sum_i I_i^r\right) \Big/ \left(\sum_i I_i^t\right). \quad (1)$$

The simple cloud model we employ neglects any contribution from the submicron haze, because the large temporal and horizontal variability in haze optical depth at the levels observed by OCPP polarimetry (Kawabata *et al.*, 1980, 1982) precludes any attempt to define either a "standard" haze-cloud model valid at all times and locations or separate equatorial and polar cloud models. To estimate the range of behavior, we also used a pure submicron haze model to normalize a subset of the images. This normalization is not ideal either, even at high latitudes where the haze is thickest, because the disk-integrated brightness is heavily weighted toward low latitudes, where the haze optical thickness is small. However, it does provide a basis for comparison of the effects of different scattering models. At low latitudes, the results of the two schemes differ only slightly, because errors in I^t are largely canceled by similar errors in I^d [see Eq. (1)]. However, the departures are significant in the polar regions, where no such compensation occurs. We have therefore been careful to consider our conclusions about the behavior of high-latitude regions in light of these uncertainties. We shall return to this point in Section IV.

As a final step in the processing of each image, the image pixels are sorted into $1 \times 1°$ latitude–longitude bins. Pixels for which the cosine of either solar or observer zenith angle is less than 0.15 are discarded, because errors in navigation and normalization are greatest near limb and terminator and because the increased slant path through the bright submicron and 1-μm aerosols subdues uv contrasts in these areas. The mean normalized brightness in each bin is then used to produce a rectangular latitude–longitude map of each image at 1° resolution. This largely eliminates the bias caused by the variation of resolution with distance from the subspacecraft point in each image. This data set is the basis for all the analyses to follow.

III. PERIODICITY OF UV FEATURES

Prior to Pioneer Venus, what little data we had on the propagation characteristics of planetary-scale wave disturbances at upper cloud levels came primarily from studies of Mariner 10 uv images. The latitudinal profile of zonal wind derived by tracking small cloud features in the images revealed a broad jet structure at midlatitudes in both hemispheres (Limaye and Suomi, 1981). However, the large-scale uv features appeared to exhibit a near solid-body rotation rather than being sheared out by these jets.

This led to the suggestion that the global patterns are actually the manifestation of planetary-scale waves propagating slowly relative to the winds at ~5–15 m/sec westward near the equator and ~20–30 m/sec eastward at midlatitudes (Belton *et al.*, 1976a,b). Two separate waves were proposed, but a single nonlinear wave of permanent shape has also been proposed to explain the observations (Rossow and Williams, 1979).

The conclusions drawn from Mariner 10 are tentative because wind measurements were acquired for less than 4 days and images for only 8 days, less than two rotation periods of the atmosphere at cloud levels. The OCPP data set is better suited to determining the rotation periods of large-scale features because of its length; its temporal resolution, while not as good as that of the Mariner 10 data, is sufficient to resolve periods >2 days. The comparison of the two data sets is of interest because the OCPP nominal mission cloud-tracked wind profile is very close to solid-body rotation (Rossow *et al.*, 1980), in striking contrast to the Mariner 10 profile. To characterize the large-scale wave properties, we consider both objective quantitative estimates and the more subjective visual evidence of the image patterns themselves.

A. Time Series Analysis of Large-Scale Brightness

Time series of normalized brightness, averaged over all longitudes observed in each image,[4] were assembled for the 66 days of continuous imaging for latitudes from 70°S to 59°N and were subjected to Fourier analysis, using the procedure described in Rossow *et al.* (1980). Two examples of these time series, at the equator and 45°S, are shown in Fig. 1. The resulting power spectrum estimates were averaged logarithmically over 20° latitude bands starting at 70°S to increase statistical significance and isolate large-scale features. The shortest resolvable (Nyquist) period is 2 days, twice the temporal resolution. The longest resolved time scale is identical to the length of the data set, 65 days [prewhitening reduces the length of the original data set by 1 day; see Rossow *et al.* (1980)].

The statistical significance of peaks in the spectra can be determined by comparison to the power levels of an appropriate spectrum which estimates the background power remaining in the absence of any periodicities. Since images on adjacent days are significantly correlated with each other, a white noise spectrum is not appropriate. Instead, a red noise continuum, which represents the characteristics of time series with both persistence and randomness, was used (Bartlett, 1960; Mitchell, 1966). The "raw" spectral estimates have 2 degrees of freedom apiece. Averaging of power over 20° latitude bands was estimated to further increase this by a factor of at least 2, since time series at adjacent latitudes are neither perfectly correlated nor completely independent. Confidence levels were finally

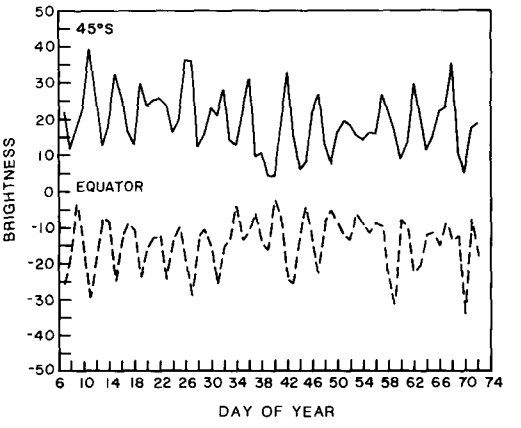

FIG. 1. Two examples of nominal mission time series of large-scale normalized uv brightness used in the power spectrum analysis.

[4] Using the longitudinal average brightness ensures that only features with zonal wavenumbers <4 contribute to time variations. The variation of phase angle over 66 days only changes the averaging length scale by ~35%. Fourier analysis of brightness variations along latitude circles shows that the variations are dominated by the very largest scales (see Fig. 4; also Rossow *et al.*, 1980), so that the phase angle variation will not affect the results.

assigned by multiplying the red noise continuum by factors representing appropriate random fluctuations about this noise level for 5.2 degrees of freedom in each latitude band.[5]

The results of the time series analysis are shown in Fig. 2. The spectra contain significant peaks in all latitude bands at frequencies $n = 12–13$ and 16–17, corresponding to periods of 5.20 ± 0.2 and 3.94 ± 0.1 days, respectively (the uncertainties reflect the frequency resolution of our data set). The 3.94-day peak dominates the signal at low and high latitudes, while the 5.20-day peak has comparable or greater strength only at midlatitudes. The only other peak of any significance is at $n = 25$ (period 2.60 ± 0.05 days); this may be the second harmonic of the 5.20-day peak, which is expected for a nonsinusoidal periodicity, not a separate wave with this period. Minor peaks also occur at $n = 18–21$ and 28–30 but are either too small, irregular, or close to the Nyquist frequency to warrant attention.

The observed periodicities refer to large-scale features, since the brightness has been averaged longitudinally over the visible disk and the power averaged latitudinally over 20° bands. It is therefore of interest to compare them with the zonal wind rotation period derived by tracking small-scale cloud features (see Fig. 17 in Rossow *et al.*, 1980). A linear least-squares fit to the nominal mission mean wind rotation period profile between 50°S and 50°N gives a rotation period of 4.65 ± 0.3 days.[6] Both the 5.20-day period and the 3.94-day period are more than one standard deviation away from the wind rotation period. Interpretation of these differences is, unfortunately, not straightforward, since at least three different scenarios are capable of producing the observed results:

(1) Two planetary-scale waves, with periods $P_1 = 3.94$ days and $P_2 = 5.20$ days, were present simultaneously during the nominal mission. The discrepancies with the zonal wind rotation period represent propagation phase speeds of the waves relative to the wind. For P_1 the relative phase speed is westward 17 ± 10 m/sec at the equator and 12 ± 9 m/sec at 45° latitude, while for P_2, the relative phase speed is eastward 10 ± 10 m/sec at the equator and 7 ± 9 m/sec at 45°,[7] given the apparent zonal wavenumber 1 structure of the features (see Fig. 4). This interpretation is qualitatively similar to that of Belton *et al.* (1976a,b) for the Mariner 10 images.

(2) Only one of the waves was present at the beginning of the observation period, but its period evolved from one of the two values to the other. Tests on hypothetical data sets made up of simple sine waves suggest that, for a 66-day series, such a change in frequency with time can produce the observed spectrum if the transition occurs over a sufficiently short interval ($\leq$2 weeks).

(3) The spectral peaks reflect the long-term amplitude modulation of global features simply advected around the planet at the ambient zonal wind speed and not propagating at all. Strictly speaking, in fact, since the power at $n = 14–15$ is not below the 5% confidence level, we cannot really claim to have resolved two separate peaks, but must admit the possibility of a single

[5] The particular red noise spectrum used was the Markov continuum. The data were passed through a hanning window before Fourier analysis. This increases the number of degrees of freedom by ~30% (Blackman and Tukey, 1958); hence, our final estimate of 5.2. Deviations from the noise level were assumed to be distributed as χ^2 divided by 5.2.

[6] The uncertainty derives from the actual rms deviation of the data of 0.2 about the linear fit plus 0.1 due to differences depending on whether the data are weighted equally, by area, or by number of vectors. It is consistent with the estimated ~7 m/sec uncertainty in determining the mean velocity at any latitude (see Rossow *et al.*, 1980).

[7] The uncertainty is determined by adding the uncertainties in the wave phase velocity and the wind velocity. A least-squares fit just to the data from 50°S to 30°S gives a wind rotation period of 4.5 days. Thus, despite the large error bar, it seems reasonable to classify the 5.20-day wave as eastward propagating with respect to the wind.

broad band centered at a period of ~4.5 days. However, if we assume that the two peaks are indeed separate, then for P_1 and P_2 to be merely sidebands of a modulated advection period the required carrier and modulation periods would be

$$P_c = \frac{2}{(1/P_1 + 1/P_2)} = 4.48\ ^{+0.33}_{-0.29} \text{ days},$$

$$P_m = \frac{2}{(1/P_1 - 1/P_2)} = 32.5\ ^{+32.5}_{-10.9} \text{ days}. \quad (2)$$

P_m is exactly half the length of the data set, because frequency resolution is $n/65$ and period resolution is therefore poor at the lowest frequencies. Consequently, P_m could be anywhere from 3 weeks to several months. The important point is that P_c is consistent with the cloud-tracked wind rotation period, making modulation a possibility. Thus, even though the spectrum of brightness variation has a deficit of power at periods ≥2 weeks (Fig. 2), other types of variations might be occurring on these longer time scales.

The second of these three possibilities seems the least likely, because there is no obvious frequency shift in time series such as those in Fig. 1. At 45°S, 12 brightness minima can be counted in 62 days, giving an average period of 5.2 days, while 16 minima occur over 63 days at the equator, for a 3.9-day period. This suggests that the spectral peaks reflect two distinct planetary-scale disturbances. However, there is some suggestion, at least at 45°S, of beats in the brightness record with an ~1-month time scale, implying an amplitude modulation period just within the uncertainties of P_m. On balance, it is not certain from this analysis alone whether two propagating waves are present or whether the long-term modulation of a simple advecting pattern is occurring. Fortunately, other lines of evidence distinguish between these two alternatives.

B. Four-Day Composite Images

In some ways the best indicators of brightness variations are the images themselves, because pattern recognition can provide a kind of "ground truth" for the results of objective analyses. We therefore constructed a series of 12 latitude vs time composite images (Fig. 3), each covering one 4-day cycle and spanning latitudes 70°N–70°S, from the normalized mapped image data set. The width of each image segment is determined by the time interval between the centers of consecutive images and the assumption that the large-scale cloud features rotate with a 4.0-day period, consistent with the dominant periodicity deduced above. The procedure is similar to that used by Belton *et al.* (1976a) on the 8 days of Mariner 10 imaging of Venus. To the extent that this assumption is valid and the large-scale clouds do not evolve dramatically in ≲4 days, the composites can be thought of as rectangular projection "maps of the world" for the uv features and provide a convenient 48-day history of the evolution of large-scale cloud albedo patterns. Latitude-dependent rotation rates based on cloud-tracked wind profiles and the dominant period at each latitude in the time series analysis results were also experimented with, as well as cross-correlation techniques for determining image boundaries, but none of these dramatically improved the visual appearance of the composite images or changed the qualitative features discussed below.

One striking feature of Fig. 3 is the reappearance of the dark equatorial band on the first day of each cycle. The details of the band morphology change from one cycle to the next, but in general this is the most stable feature in the images. It is obviously the cause of the dominant 3.94-day peak in the low-latitude time series power spectra. The last 2 days of each cycle are characterized by large tilted bow shapes and/or V- or Y-like features, but these are more ephemeral. At midlatitudes, the brightness variation is dominated by the bright polar bands, one in each hemisphere, which oscillate in latitudinal position between ~45 and 55° (Rossow *et al.*, 1980). A comparison between

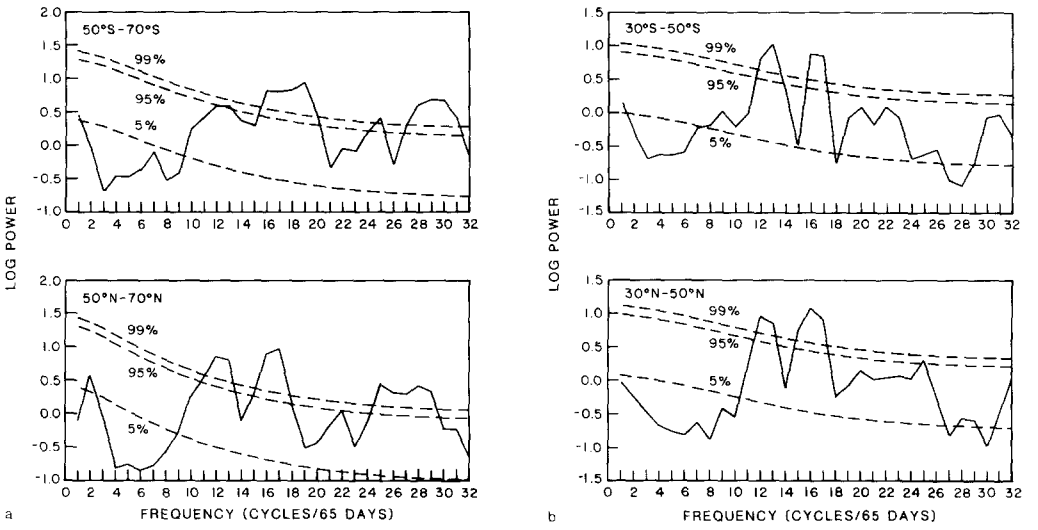

FIG. 2. Power spectra of time series, such as those in Fig. 1, averaged logarithmically over 20°-wide latitude bands. The dashed lines represent confidence levels for the statistical significance of spectral peaks or deficits based on comparisons with a Markov red noise continuum assuming 5.2 degrees of freedom. Latitude bands in each hemisphere: (a) 50–70°, (b) 30–50°, (c) 10–30°, (d) 10°N–10°S. The 50°N–70°N band actually contains no data poleward of 59°N due to gaps in coverage on certain days.

adjacent composite images, however, shows that the bands oscillate with a period of ~5 days rather than ~4 (Fig. 3c illustrates this particularly well). This is compelling evidence for the authenticity of the 5.20-day peak, which is strongest in the midlatitude power spectra. We therefore conclude that the two spectral peaks reflect real propagating waves.

Feature discontinuity across image boundaries indicates changing conditions, either in the zonal flow speed or simply in the clouds themselves. In several instances, most notably Days 39–42 and 47–50, features can be traced easily from one image to the next, and obvious Y-like features are seen. At other times, though (e.g., Days 27–30 and 55–58), compositing produces poorer results. In these images, periodicities are difficult to discern, yet the progression of features in subsequent cycles remains in phase with that of previous cycles. This suggests that the cloud "tracer" is changing and not the dynamics. Thus the amplitude fluctuations in Fig. 1 may merely reflect variations in the upper cloud structure.

It remains to determine the longitudinal structure of the waves. The general continuity of the composite images suggests that both the equatorial band and the bright polar bands are zonal wavenumber 1 perturbations. This has been noted previously on the basis of Mariner 10 data (Belton *et al.*, 1976a,b). On the other hand, the Y feature has at times been interpreted as wavenumber 3 (Dollfus, 1975) and the bright polar bands as wavenumber 2 (Suomi and Limaye, 1978). Unfortunately, Fourier analysis of individual images can only resolve scales as large as planetary wavenumber 3, since less than half of any latitude circle is observed. We can remove this constraint by using the mosaics to represent a complete range of longitude, albeit at the cost of additional noise due to the discontinuities between adjacent images and to scattering geometry variations over the orbit not adequately removed by the normalization scheme.

Figure 4 shows the power spectra obtained by Fourier analyzing the intensity values in each completely filled composite latitude circle and then averaging the power

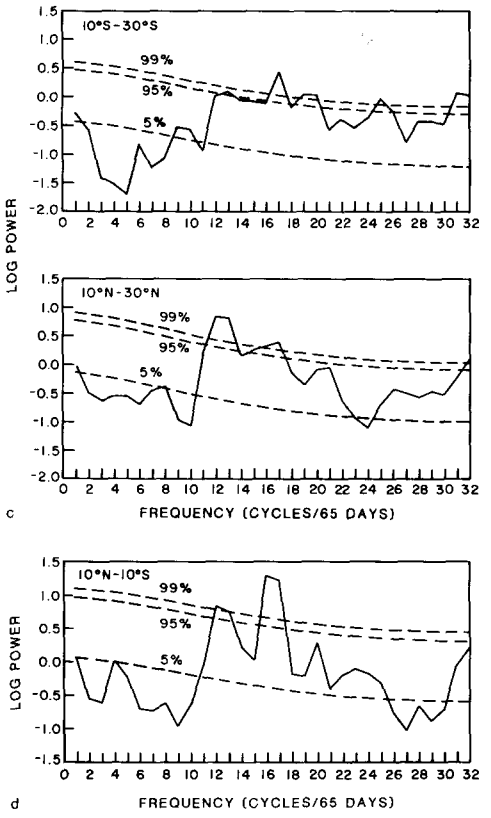

FIG. 2—*Continued.*

logarithmically over 20°-wide latitude bands and over all 12 composites. The spurious power is concentrated at wavenumber 4 and all its harmonics, because the spacecraft orbital period is one-fourth the length of the composite, and the artifacts are quasi-periodic but not sinusoidal. Despite this, wavenumber 1 dominates the spectrum in every latitude band. This verifies the impressions of Belton *et al.* (1976a,b) about the longitudinal structure of the large-scale features. It is also consistent with expectations if the dynamics of Venus' stratosphere are roughly two-dimensional and vorticity conserving (Rossow and Williams, 1979). When forcing for the flow is weak, inertial nonlinear interactions dominate, and energy cascades from high to low wavenumbers. Given Venus' slow rotation rate, the cascade can proceed up to the very largest scales. There is no sign of wavenumber 2 or 3 dominance.

We therefore propose the following explanation of all the observations. Two distinct planetary-scale waves, centered at different latitudes and propagating in opposite directions relative to the zonal wind, were present during the Pioneer Venus nominal mission. The periods and phase speeds are those calculated in part A of this section. Both waves have a zonal wavenumber 1 structure and are symmetric about the equator, as suggested by Figs. 2 and 3, but the latitudinal widths of the two differ. The 3.94-day wave, centered on the equator, is global in extent, while the 5.20-day oscillation, centered at ~45–55° latitude, is more confined meridionally. Both waves appear to be present throughout most of the 66-day imaging period. The interaction between the two waves in midlatitudes apparently results in long-period variations, as will be seen in Section IV.

C. High-Pass-Filtered Composite Images

Thus far we have discussed the behavior of large-scale features exclusively, but the images also contain a wealth of interesting small-scale details. To isolate these features, we digitally high-pass filtered some of the composite images (Fig. 5). First, the intensities were smoothed using a normalized two-dimensional 13-point Gaussian function with standard deviation $\sigma = 2°$. The smoothed intensities were then subtracted from the originals ($I_{i,j}$) to give the intensities ($I_{i,j}^{h}$) of the high-pass-filtered images:

$$I_{i,j}^{h} = I_{i,j} - \frac{1}{2\pi\sigma^2} \sum_{m=i-6}^{i+6} \sum_{n=j-6}^{j+6} I_{m,n} \exp \frac{-[(m-i)^2 + (n-j)^2]}{2\sigma^2}. \quad (3)$$

The half-power point of this filter is near wavenumber 34, so features with spatial scales $\lesssim$ 1100 km are subdued in Fig. 5.

Small-scale features fall into two general classes described by Rossow *et al.* (1980). Cellular features dominate the structure at low latitudes. These may be the manifestation of small-scale convection at visible cloud levels or below. Elsewhere the preferred morphology is a streak texture which

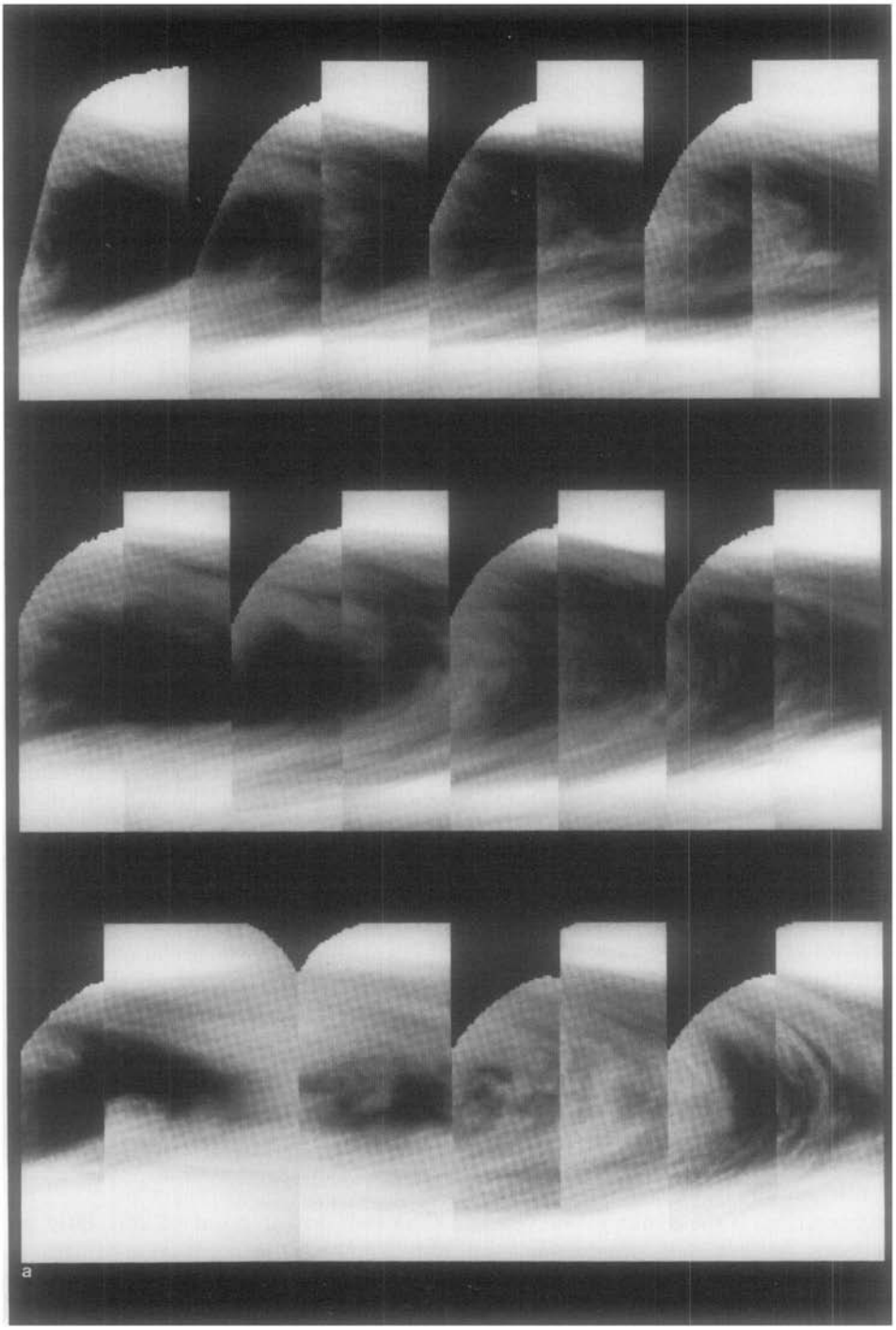

FIG. 3. Four-day latitude vs time composite uv images spanning latitudes 70°N–70°S and covering 48 days in 1979 during the nominal mission. The width of image segments is determined by the assumption that features move in longitude 90°/day. The irregularity of the upper boundaries of the images is due to variations in viewing geometry over each orbit. (a) Days of year 19–30, (b) Days 31–42, (c) Days 43–54, (d) Days 55–66.

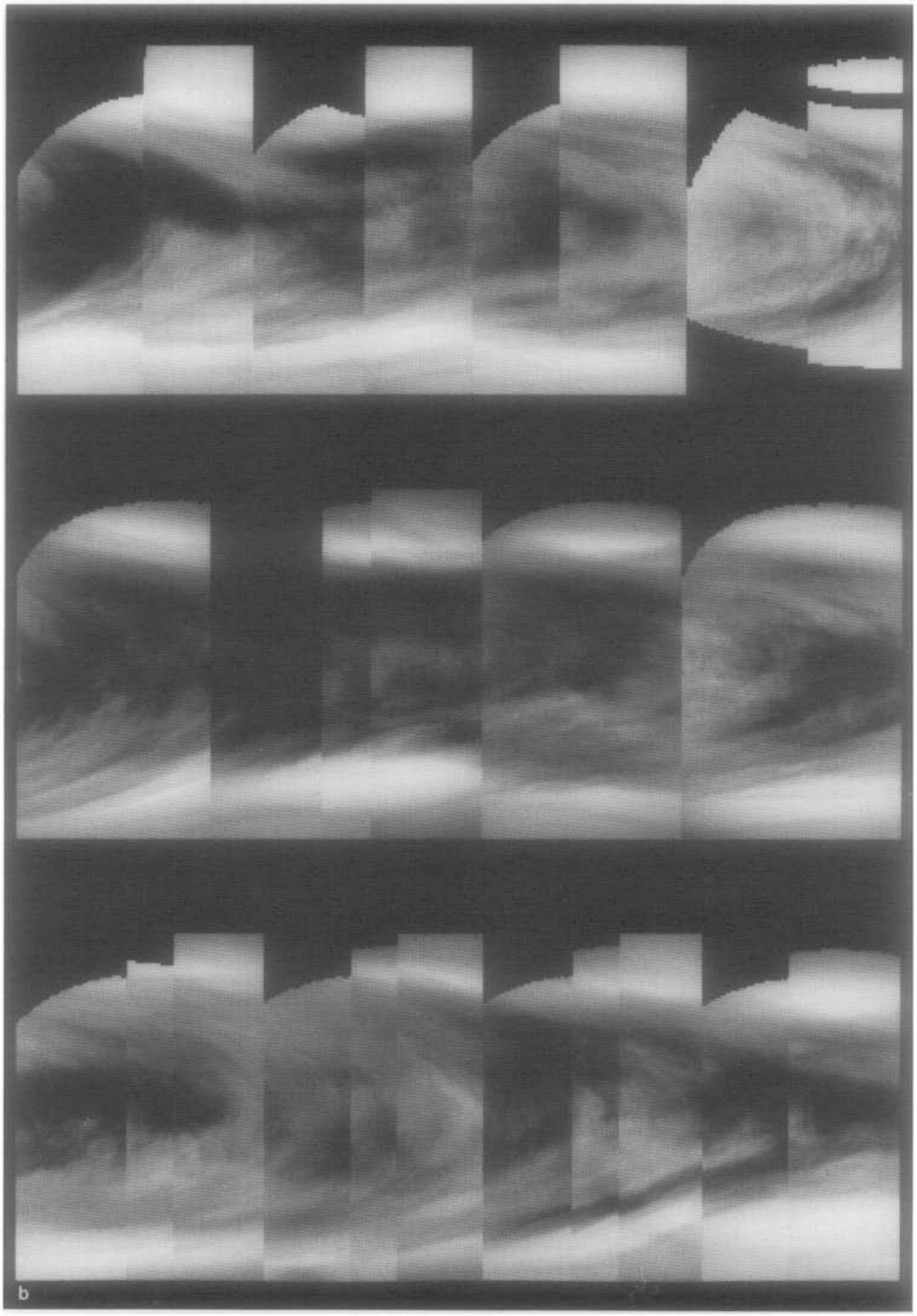

FIG. 3—*Continued.*

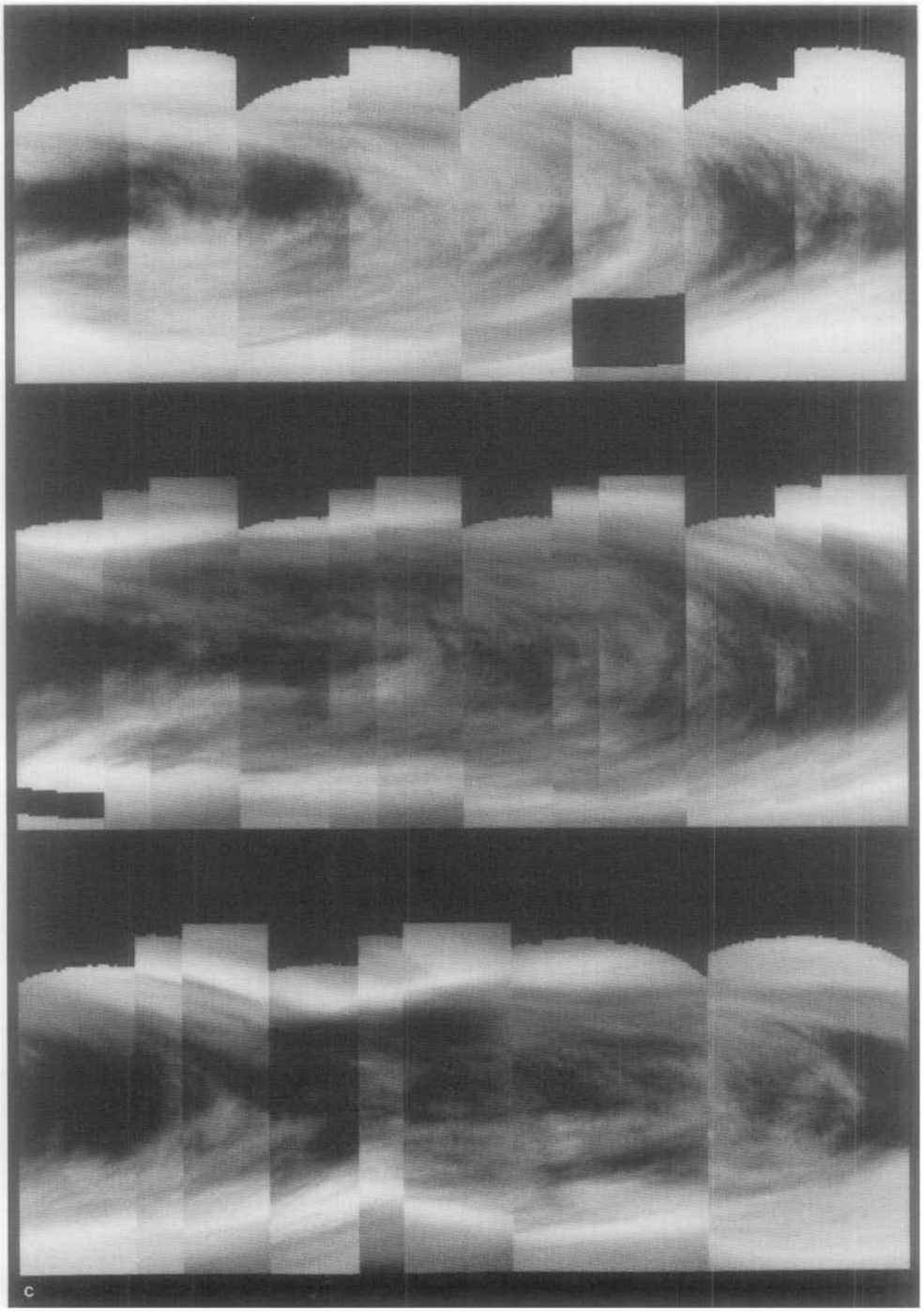

FIG. 3—*Continued.*

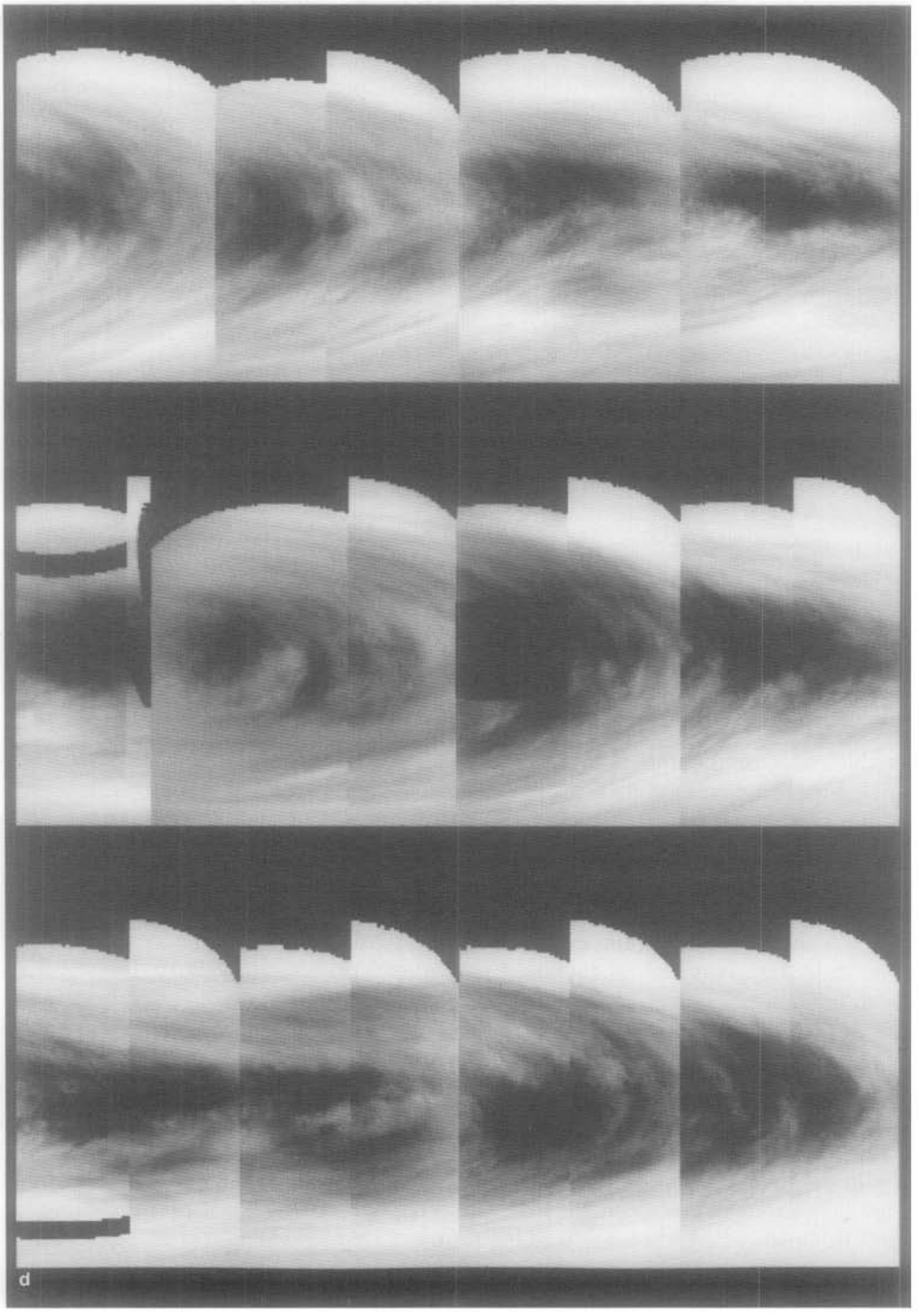

FIG. 3—*Continued.*

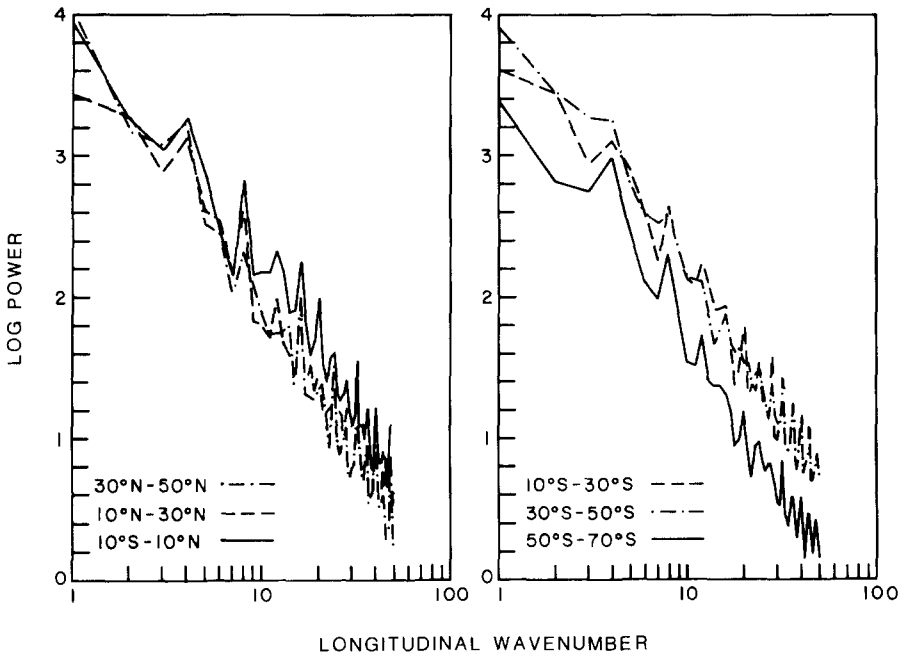

FIG. 4. Longitudinal cloud brightness power spectra of the composite images in Fig. 3 averaged logarithmically over 20°-wide latitude bands and all 12 composites. (Left) Northern hemisphere and equatorial region. (Right) Southern hemisphere.

forms the basis of the tilted bow-shaped patterns seen to some extent in every image. Each type of structure exhibits a definite correlation with the large-scale albedo patterns, as can be seen by comparing Figs. 3c and 5.

The cells are generally located in regions of large-scale dark material, occurring primarily in low latitudes when the dark equatorial band is present, but penetrating farther poleward in the vicinity of the dark arms of the Y feature. The correlation with dark material has been noted before (Belton *et al.*, 1976b; Rossow *et al.*, 1980), and two explanations have been proposed: (1) the cells are ubiquitous but most visible in dark regions because of the higher contrast there; or (2) they exist preferentially in and are physically interrelated with dark regions. The former was our initial impression (Rossow *et al.*, 1980), but based on the appearance of the composite images, we now favor the latter explanation. If cell visibility were solely dependent on contrast level, we would expect to see few small-scale features in bright regions. Instead, the transition from large-scale dark to bright, especially at midlatitudes, is marked simply by a gradual change from cellular to streak features. The contrast seems to be adequate in bright regions (except the polar bands) to reveal small features, but cells are generally not present.

Streak features are apparent in both bright and dark regions, though somewhat obscured by cellular features within the latter. Rather than albedo, they correlate with the orientation of planetary-scale markings relative to latitude circles. Comparison of Figs. 3c and 5 shows that they line up almost zonally when the dark equatorial band is present but tilt as much as 45° near the arms of the Y and larger bow-shaped features. The tilt of these streaks thus oscillates with the same 4-day periodicity as the large-scale patterns, not the 4.65-day advection period determined by tracking the translational motions of these same fea-

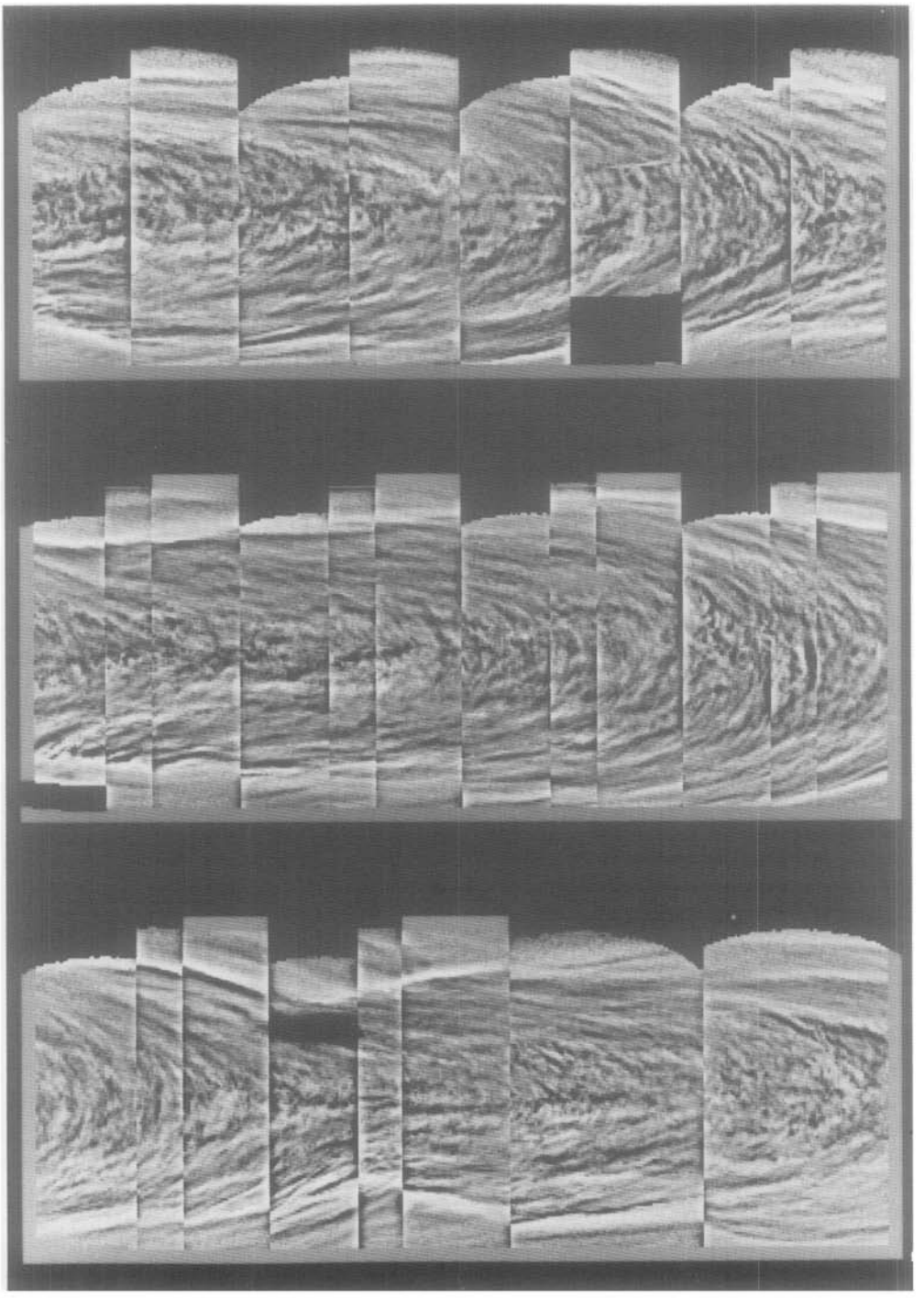

FIG. 5. High-pass Gaussian filtered version of the composite images in Fig. 3c. The filter subdues features on scales larger than ~1100 km.

tures. Again, the impression is that of a dynamical interaction between features on different scales.

IV. INTERMEDIATE AND LONGER-TERM VARIABILITY

The rotation of uv patterns dominates the signal in almost any kind of time series one constructs from OCPP image data. To reveal fluctuations on longer time scales, all of the time series discussed in this section were smoothed using 4-day equally weighted running means. This emphasizes cycle-to-cycle variations at the expense of day-to-day changes. In addition, 3- and 5-day running means were computed for several time series and compared with the 4-day running mean to ensure that the choice of smoothing interval does not bias our conclusions.

A. Single-Image Longitudinal Power Spectra

Longitudinal cloud brightness power spectra were calculated by Fourier analyzing the normalized brightness distribution along latitude circles in 114 individual images (Fig. 6). The method used was essentially that described in Rossow *et al.* (1980), with one minor difference: the longitudinal length of the data sets was restricted to a 121° segment at each latitude centered as close as possible to the subsolar meridian. This eliminates a possible source of latitudinal and temporal bias[8] and minimizes the spurious power introduced by foreshortening and slant path variation effects.

The basic features of the spectra are similar to those deduced from a preliminary subset of images (Rossow *et al.*, 1980). The only real peak occurs at or below the lowest resolved wavenumber ($k = 3$). There exists a "kink" in the spectrum at approximately wavenumber 10 in all latitude bands. The slopes of the spectra, as determined by least-squares linear fits, generally increase in magnitude (i.e., the spectra steepen) with increasing latitude (see Table I) at the lower wavenumbers. This is exactly opposite the latitudinal variation in slope determined by Travis (1978) from Fourier analysis of 2 days of Mariner 10 images.

TABLE I

TIME MEAN LONGITUDINAL CLOUD BRIGHTNESS POWER SPECTRUM SLOPES

Latitude band	Wavenumber range				
	5–50	5–10	10–20	20–30	30–50
50°S–70°S	−2.91	−5.63	−3.10	−2.38	−1.74
30°S–50°S	−2.67	−3.91	−2.64	−2.49	−2.51
10°S–30°S	−2.44	−3.23	−2.83	−1.86	−2.18
10°N–10°S	−2.40	−3.07	−2.40	−2.55	−2.08
10°N–30°N	−2.35	−3.92	−2.04	−2.63	−1.64
30°N–50°N	−2.98	−4.31	−2.96	−2.27	−3.12

This difference can be explained by significant temporal variability in the cloud feature size spectrum. We plotted the spectral slope in the wavenumber range 10–20 vs time (Fig. 7) and indeed found that the fluctuations can be quite large (>1) at all latitudes. At certain times, in fact, the slope magnitude decreases with latitude (e.g., Days 30–31), as it did at the time of Mariner 10 observation. Of particular interest is the quasi-periodic variation of slope at latitudes 30°S–50°S with an apparent time scale of 2–3 weeks (Fourier analysis of this time series yields a peak at 19 ± 3 days). The visual manifestation of this periodicity is an apparent fluctuation in strength of the large (zonal wavenumber ~ 20) bow-shaped features associated with the Y, as can be seen from Fig. 3. For example, the slope magnitude is at or near a minimum on Days 34, 50, and 66, and the images on these days are dominated by numerous large, high-contrast bow shapes. In between (e.g., Days 26, 42, 58), when the slope is maximum, the images contain less bow-shaped activity and Y features are more zonally oriented and latitudinally confined.

In the former case, the V- or Y-shaped features coincide with the highest latitudinal extent of the bright polar bands, while in

[8] The images selected are all at low enough phase angles so that 121° of longitude are observable.

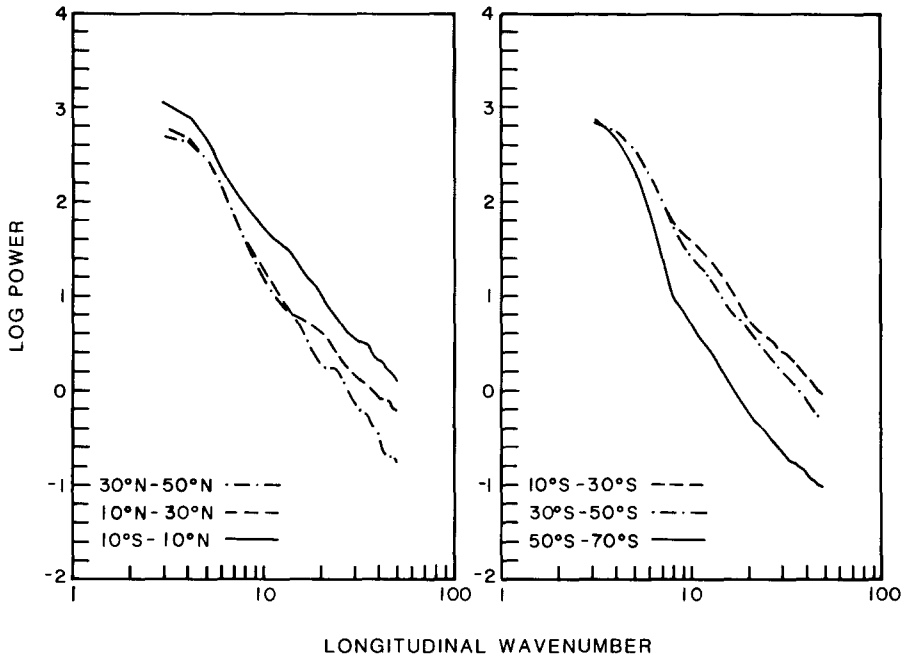

FIG. 6. Longitudinal cloud brightness power spectra averaged logarithmically over 114 individual images and 20°-wide latitude bands. (Left) Northern hemisphere and equatorial region. (Right) Southern hemisphere.

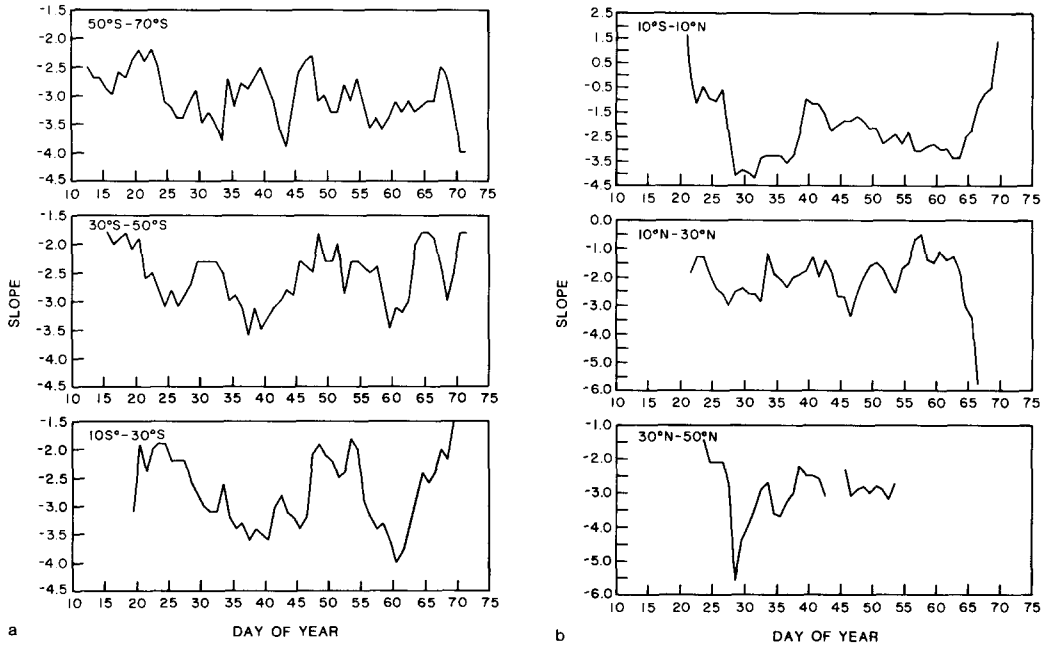

FIG. 7. Time series of single-image longitudinal cloud brightness power spectrum slopes in the wavenumber range 10–20, smoothed by a 4-day equally weighted running mean. (a) Southern hemisphere, (b) equatorial region and northern hemisphere.

the latter case the bands are furthest equatorward when tilted features appear at low latitudes. Therefore, the periodicity may reflect a $\frac{4}{3}$ "commensurability" between the 3.94- and 5.20-day waves discussed in Section III. In other words, the bow-shaped features may be the result of a dynamical interaction between eddies in low and midlatitudes. Alternatively, the bow shapes may merely represent the addition of overlapping wave amplitudes at varying relative phase, analogous to the suggestion of Belton *et al.* (1976b) for the Y feature. In either case, it implies that the two propagating waves exist at the same level even though we see to different depths in equatorial and midlatitude regions. Unfortunately, data in the 30°N–50°N latitude band are too sparse to reveal whether a similar variation exists there simultaneously.

Systematic fluctuations in slope occur at other latitudes, but with different time scales. For example, at 10°S–30°S and 10°N–10°S a 20- to 30-day periodicity is suggested. The cause of this behavior is not evident, although it roughly correlates with the time interval over which recognizable Y or V features persist (Fig. 3). Elsewhere, no obvious periodic behavior occurs.

Nonetheless, at all latitudes, a strong negative correlation exists between the spectral slopes at low and intermediate wavenumbers. Table II presents cross-correlation coefficients between the time series of slopes in three wavenumber ranges for six latitude bands. The large negative correlations throughout the first column of this table demonstrate that the slope increases at low wavenumbers while decreasing at intermediate wavenumbers, and vice versa, that is, the spectrum flexes about a pivot point near wavenumber 10. This flexing can result in a spectral shape similar at times to that derived by Travis (1978). The variation in shape could be due either to sporadic injection of power near wavenumber 10 or to simultaneous forcing at low ($k < 10$) and intermediate ($10 < k < 20$) wavenumbers. We favor the latter, because the spectrum is generally much steeper at larger scales than at intermediate scales (see Table I). In other words, the kink at wavenumber 10 reflects a relative deficit of power there rather than a relative excess. The slope at high wavenumbers, in contrast, does not correlate especially well with that at either low or intermediate wavenumbers, except in the equatorial region, where it is correlated with the former and anticorrelated with the latter. This is further evidence for contemporaneous forcing at large and intermediate scales. Regardless of whether the cloud brightness spectrum reflects the spectrum of eddy kinetic energy or some other quantity, our results suggest coordinated interactions between features on very different spatial scales.

TABLE II

CROSS-CORRELATION COEFFICIENTS BETWEEN POWER SPECTRUM SLOPES IN VARIOUS WAVENUMBER RANGES

Latitude band	Wavenumber ranges		
	5–10/10–20	10–20/20–30	5–10/20–30
50°S–70°S	−0.38	−0.51	+0.12
30°S–50°S	−0.30	−0.11	−0.11
10°S–30°S	−0.74	−0.01	−0.16
10°N–10°S	−0.57	−0.74	+0.62
10°N–30°N	−0.57	−0.16	+0.04
30°N–50°N	−0.54	−0.17	−0.00

B. Disk-Integrated Intensity

The normalization factor described in Section II is also a good approximation to the total intrinsic brightness of Venus at $\lambda = 365$ nm as observed from a large distance. Its temporal variation is dominated by the 4-day quasi-periodicity of the dark horizontal Y. However, after multiple smoothing with a 4-day running mean, variation on longer time scales is revealed (Fig. 8).

Two types of variability are present in this figure. The dominant feature is a general monotonic decrease in brightness over the length of the record, which could imply a vacillation of global brightness on a time

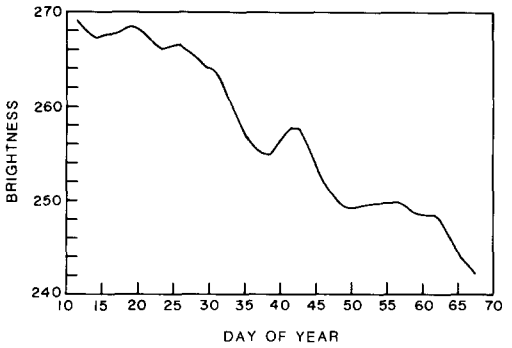

FIG. 8. Time series of the disk-integrated uv brightness of Venus, smoothed by three successive applications of an equally weighted 4-day running mean.

scale greater than 2 months.[9] Kawabata *et al.* (1982) do in fact observe a systematic decrease in polar haze optical thickness on time scales of several hundred days. However, our view of Venus shifted gradually from the morning quadrant to the afternoon quadrant during the nominal mission, so that a solar-locked longitudinal variation of brightness, with the afternoon side being darker than the morning, can also explain this observation. The nominal mission data alone do not permit us to distinguish between temporal and fixed longitudinal dependence of the disk brightness.

Superimposed on this trend is a small-amplitude oscillation with a periodicity of about 2–3 weeks. Once every ~15–20 days the dark Y feature or its equivalent is in view at the same time that the bright polar bands are farthest poleward and most foreshortened (see Fig. 3). Because the disk-integrated brightness is usually weighted toward low latitudes due to foreshortening and the nature of the Pioneer Venus orbit, on these days (e.g., 38, 50, 66) the disk brightness is at a local minimum. This may be a manifestation of beating between the 3.94- and 5.20-day planetary-scale waves.

[9] OCPP observations are calibrated by observing both an internal calibration lamp and an external diffuse target illuminated by the Sun. Variations of instrument response are small compared to the variations discussed here.

C. Longitudinally Averaged Normalized Brightness

Time series like those in Fig. 1 exhibit several types of variability, but underlying long-term changes are difficult to see in the presence of the 3.94- and 5.20-day signals. Figure 9 shows the longitudinally averaged normalized brightness vs time after smoothing in time and averaging over 20°-wide latitude bands. Of particular interest is the strong ~2-month brightness fluctuation in both polar regions (50–70° in each hemisphere and to a lesser extent at 30°N–50°N). Part of this variation is an artifact resulting from our use of a pure 1-μm aerosol model for normalization. The phase function [and therefore I^t in Eq. (1)] for 1-μm particles at $\lambda = 365$ nm is greater at small phase angles than that for the $\frac{1}{4}$-μm particles which actually dominate at high latitudes, but it drops off more sharply and becomes smaller than the $\frac{1}{4}$-μm phase function at intermediate phase angles (Hansen and Travis, 1974). Therefore, a 1-μm normalization introduces an artificial monotonic trend of the normalized brightness with increasing phase angle in the polar regions (0° phase angle occurs on Day 44).

To study this, we normalized a subset of the images covering a wide variety of phase angles using a cloud model for a pure $\frac{1}{4}$-μm haze. The amplitude of the fluctuation decreased (~50%) but was not eliminated, because the observed variations are oscillatory in nature rather than monotonic functions of phase angle. We therefore conclude that some of the variability is real and we are seeing the poles brighten and darken on an ~2-month time scale. This behavior is consistent with ground-based observations of polar brightening events (Dollfus, 1975). OCPP polarimetry may also indicate a concurrent variation in polar haze optical depth (Kawabata *et al.*, 1982).

At lower latitudes, long-term brightness variations relative to the disk-averaged intensity are much smaller and more irregular. Near the equator, especially, no trend

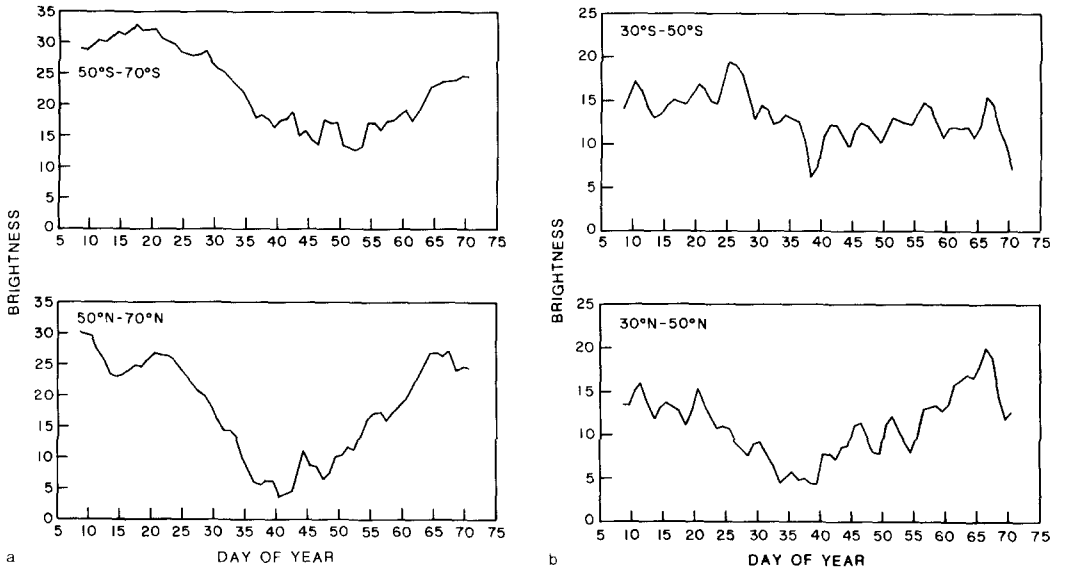

FIG. 9. Time series of zonal mean normalized uv brightness averaged over 20°-wide latitude bands and smoothed by an equally weighted 4-day running mean. Latitude bands in each hemisphere: (a) 50–70°, (b) 30–50°, (c) 10–30°, (d) 10°N–10°S.

is obvious. However, at 10°S–30°S we observe an ~2-month fluctuation almost exactly out of phase with that at 50°S–70°S; that is, while high latitudes darken, a region at lower latitudes brightens, and vice versa. It is tempting to suggest that these two phenomena are connected. On the other hand, the evidence for similar behavior at 10°N–30°N is poor by comparison. Of course, the north pole was somewhat darker than the south pole during the nominal mission (Fig. 9 and Rossow *et al.*, 1980) so there may have been less haze available in northern latitudes to produce such an effect. Data from several more imaging periods should reveal whether the variability reported here is systematic and repeatable or not.

V. DISCUSSION

The previous sections demonstrate that the Venus clouds undergo highly complex brightness variations on time scales ranging from a few days to a few months or longer. Our difficulty in qualitatively describing changes in the uv appearance of Venus (Rossow *et al.*, 1980) largely stems from this intermingling of time scales. Although we do not know which dynamic state variable we observe, the variations suggest some properties of the dynamics near the cloud tops. The following ideas should be considered as hypotheses to be tested against the results of future analyses.

Some insight into the nature of the waves we observe may be gained by considering the possible instability mechanisms which can produce waves on Venus. If the stratospheric dynamics are roughly two-dimensional and vorticity conserving (Rossow and Williams, 1979), planetary-scale advection waves (Thompson, 1948) should be common. Advection waves are the generalization of Rossby–Haurwitz waves on a slowly rotating planet, advecting mostly relative rather than planetary vorticity. One mechanism for generating such waves is barotropic instability (cf. Kuo, 1949). Two features of neutral and unstable barotropic waves are significant in light of our observations of brightness variability. (1) Since

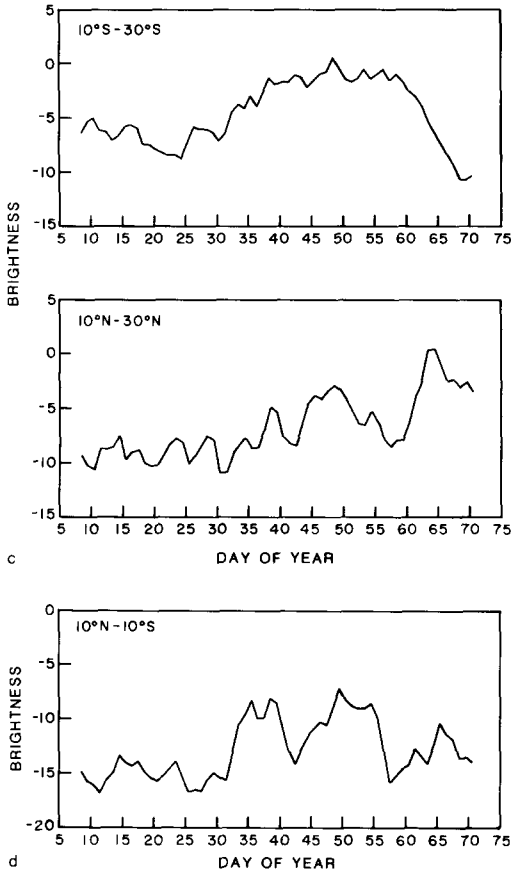

FIG. 9—*Continued.*

an unstable disturbance acquires its kinetic energy from that of the mean flow by transporting momentum out of and smoothing out a jet, the streamlines of a barotropically unstable perturbation are tilted in a direction opposite to the sense of the gradient of the *angular* velocity of the mean zonal flow. A neutral wave perturbation, on the other hand, is not tilted and therefore does not transport momentum latitudinally. (2) The phase speed of an unstable disturbance is slower than the zonal flow speed at the point where the absolute vorticity has an extremum but is faster than the minimum speed of the zonal flow. A neutral wave phase speed is less than the minimum flow speed if no absolute vorticity extremum exists, but if an extremum is present, a neutral perturbation can also have a phase velocity which matches the flow velocity at the point of extremum.

The Mariner 10 cloud-tracked wind profile contained midlatitude jets with a maximum in absolute vorticity at 48°S latitude (Travis, 1978), thus satisfying Rayleigh's criterion, one of two necessary conditions for barotropic instability. The absence of these jets in Pioneer Venus nominal mission cloud-tracked winds suggests that barotropic instability may have acted to produce the more stable Pioneer Venus wind profile (Rossow *et al.*, 1980). The 5.20-day latitudinal oscillation of the bright polar bands at midlatitudes has a phase speed which appears to be somewhat slower than the zonal flow; its apparent wavenumber 1 structure implies that it is the product of a nonlinear energy cascade from high to low wavenumbers. Therefore, we suggest that the 5.20-day periodicity represents a neutral global-scale advection wave which evolved by two-dimensional processes from a previously barotropically unstable flow at cloud levels. The morphology of the bands corresponds most closely to the streamfunction of the total flow [cf. Figs. 4 and 5 in Rossow and Williams (1979) for an example]. In other words, the bright material at midlatitudes appears to trace the flow field directly. The eastward relative propagation of the midlatitude wave is consistent with that deduced from the Mariner 10 images, despite the large difference in midlatitude wind velocities at these times, but a detailed comparison is not possible due to the short duration of the Mariner 10 observing period.

The 3.94-day equatorial wave, which is presumably the same phenomenon observed in the Mariner 10 images, may be different in character from the oscillation at midlatitudes. It does not appear to be an advection wave, since it propagates significantly faster than the zonal flow at all latitudes. The longitudinal structure of Mariner 10 cloud-tracked zonal eddy velocities (Limaye and Suomi, 1981) suggests that the

band may be a region of flow divergence.[10] If the meridional eddy velocities measured by Limaye and Suomi (1981) are correct, their nonzero values near the equator preclude a Kelvin wave interpretation of the equatorial band, as suggested by Belton *et al.* (1976b). However, it is still possible that some type of gravity wave (Covey and Schubert, 1981) is responsible for this feature. The forcing mechanism for the equatorial band is not obvious from the image data, although the correlation of cells with the band (Figs. 3c and 5) suggests a possible forcing by mesoscale convection. Alternatively, the convection might be stimulated by temperature perturbations associated with dark material either indirectly due to the wavelike nature of the band or directly via radiative feedback in areas of strong uv absorption.

Information from other Pioneer Venus experiments may shed light on the vertical propagation characteristics of these waves. Nominal mission time series of infrared brightness temperature in four sounding channels acquired by the Orbiter Infrared Radiometer (OIR) have been Fourier analyzed by Apt and Leung (1982) and found to contain a primary peak at 5.3 ± 0.4 days at high and midlatitudes. This may reflect the same phenomenon we see at midlatitudes in the uv. The phase of this wave appears to vary with height, suggesting vertical propagation (Taylor *et al.*, 1980). However, the 4-day oscillation so obvious in the uv is not seen at all by the OIR, which views levels higher than those represented by the uv features. This may mean that the 3.94-day wave does not propagate vertically, while the 5.20-day wave does. The 3.94- and 5.20-day waves propagate faster and slower than the mean zonal wind at cloud levels, respectively. Thus, if the zonal wind continues to increase in magnitude throughout and above the clouds (where its structure is presently unknown), the 3.94-day wave would soon reach a critical level, where its phase speed matches the wind speed, and be absorbed or reflected there, while the 5.20-day wave would not. Because the zonal wind decreases monotonically with depth below uv cloud levels (cf. Counselman *et al.*, 1980), the critical level for the latter wave is at ~55–60 km altitude, below the region we see, so it could propagate freely if generated above this level. The barotropic instability explanation of the 5.20-day wave is consistent with this constraint, because in this scenario the perturbation is forced locally by momentum transport along the poleward branch of the cloud-level Hadley cell.

The large bow-shaped features [see Rossow *et al.* (1980) for definition] are particularly intriguing, because of their characteristic tilt, symmetry, and sporadic nature. The ~4-day periodicity of these features (Fig. 3) seems to indicate that their origins are tied to the dark equatorial band. The ~2- to 3-week quasi-periodicity in their strength suggests that this comes about via a dynamical interaction between the 5.20- and 3.94-day waves, although it is possible that a simple beat phenomenon involving the two overlapping waves can in some way explain the observed morphology. The large-scale pattern is reminiscent of a barotropically unstable disturbance, but one occurring at low latitudes. If the tilt of the large bow shapes implies instability, the associated eddy momentum transport would be poleward in both hemispheres, and this might be manifested by the varying tilt of the small streak features. Such a transport was calculated in cloud-tracked winds by Limaye and Suomi (1981) over 3 days of Mariner 10 imaging, when bow shapes were prominent. However, this eddy transport was much smaller than, and of the wrong sign to balance, the transport by the mean meridional circulation, so the bow shapes may not play a primary role in the momentum balance. If barotropic instability is re-

[10] Conclusions about eddy velocities should be viewed as tentative because of the uncertainties involved in determining individual cloud-tracked wind vectors and in defining the zonal mean flow from the short Mariner 10 observing period.

sponsible for smoothing out midlatitude jets built up by the meridional circulation on Venus, then at times of instability we can instead expect to observe large equatorward eddy momentum transports and different uv feature characteristics. The features seen in the nominal mission images may represent only one stage in the variation of the dynamics and cloud features of Venus. Until we observe an instability in progress and can correlate the disturbance with the uv features, we must regard these ideas as speculative.

The observed ~2-month oscillation of polar brightness also has possible implications for the dynamical balances in the Venus stratosphere. Rossow *et al.* (1980) suggested that the rapid zonal wind at cloud levels is a consequence of a vacillation cycle involving momentum transport by a mean meridional circulation and quasi-barotropic eddies. They further suggested in that paper that ground-based observations of occasional polar brightening (Dollfus, 1975) might be caused by this vacillation as follows. Quasi-barotropic eddy parcel exchanges would mix bright submicron haze particles into low latitudes and somewhat less bright 1-μm H_2SO_4 droplets into high latitudes when eddies were active, thus darkening the pole. When eddies were dissipating, haze would build up at high latitudes, thereby brightening the pole. Our results tentatively support this interpretation, for two reasons: (1) the time scale we observe for the polar brightness variation is consistent with that suggested for the vacillation cycle (Rossow and Williams, 1979; Rossow *et al.*, 1980); (2) the brightness variation at 10°S–30°S, which is out of phase with that at 50°S–70°S, suggests that lower-latitude brightening is tied to polar darkening. Suggestions of polar haze optical depth fluctuations deduced from OCPP polarimetry (Kawabata *et al.*, 1982) may also correlate with this behavior. However, the verification of this connection between polar brightening and vacillation of the zonal flow will depend ultimately upon the observation of temporal variations in eddy kinetic energy levels and momentum transports from cloud-tracked wind measurements.

VI. SUMMARY

The observed temporal variability of ultraviolet cloud brightness in over two months of Pioneer Venus OCPP imaging can be characterized as follows:

1. The longitudinal mean brightness record shows evidence of two planetary-scale waves. One appears to be centered on the equator but has significant amplitude at all latitudes. It has a period of 3.94 ± 0.1 days and propagates westward relative to the mean zonal flow at an equatorial phase speed of 17 ± 10 m/sec. The other is centered at midlatitudes and is more confined latitudinally, has a period of 5.20 ± 0.2 days, and propagates eastward relative to the zonal wind with a phase speed of 7 ± 9 m/sec at 45° latitude. Visually, the two waves correspond to the longitudinal motion of the dark equatorial band and the oscillation in latitude of the bright polar bands, respectively.

2. The slope of the longitudinal cloud brightness power spectrum at intermediate wavenumbers fluctuates with a periodicity of ~2–3 weeks in southern midlatitudes. This appears to coincide with variations in the strength of large bow-shaped features in the images. The ratio of the periods of the dark equatorial band and bright polar bands suggests a dynamical interaction between the two being responsible for this phenomenon.

3. The polar regions in both hemispheres vary in brightness on a time scale of ~2 months. This is consistent with ground-based observations of sporadic polar brightening and with the inferred advection time scale of the mean meridional circulation at cloud levels.

4. The disk-integrated brightness decreased with time throughout the nominal mission. It cannot yet be determined whether this represents a real time variation

or a solar-locked longitudinal dependence of brightness.

5. Small-scale feature behavior correlates with the large-scale albedo patterns. Specifically, cellular features exist primarily where large-scale dark material is present, despite adequate uv contrast elsewhere. In addition, the orientation of streak features with respect to latitude circles oscillates with the same ~4-day periodicity as the large-scale features at low latitudes.

Our conclusions must be regarded as tentative, since they are based on an analysis of only ~2 months of uv feature contrasts whose physical nature is not yet understood. The numerous time scales present in the data only underscore the possible complexity of the dynamical regime and emphasize the need for continuing observations covering many hundreds of days. Existing and future Pioneer Venus extended mission data should partly alleviate this deficiency, but even so, there is no guarantee that we will ever be able to understand all of the operative eddy–mean flow interactions underlying the general circulation of the Venus stratosphere by utilizing observations alone. To proceed further, extensive numerical modeling of Venus-like fluids is necessary, from fully three-dimensional general circulation models to simple barotropic two-dimensional models. By studying the spatial and temporal variability of the eddy transports, energy conversions, and jet formation and destruction in such idealized turbulent fluids, we can better understand the processes responsible for the present dynamical state of the Venus atmosphere.

ACKNOWLEDGMENTS

The authors wish to thank Kiyoshi Kawabata for providing his fast invariant imbedding routine for normalization, Ed Kinsella for providing nominal mission digital cloud-tracked wind data, and Larry Travis for the use of his image navigation scheme. We acknowledge Scott Davis, Lex Lane, Sanjay Limaye, Roger Opstbaum, Peter Stone, and Larry Travis for numerous helpful discussions. Several preliminary analyses of the image data were carried out by Linda Berens, Eileen Cupta, and Stephen Jensen during their participation in the Summer Institute on Planets and Climate at the Goddard Institute for Space Studies and Columbia University. We are also grateful to George Bier for assistance with image data processing, Patrice Palmer for photographic processing of images, Lilly Del Valle and Jose Mendoza for preparing graphics, and Beth Duckett and Elizabeth Porto for typing the manuscript.

REFERENCES

APT, J., AND J. LEUNG (1982). Thermal periodicities in the Venus atmosphere. *Icarus* **49,** 427–437.

BARTLETT, M. S. (1960). *An Introduction to Stochastic Processes*. Cambridge Univ. Press, New York.

BELTON, M. J. S., G. R. SMITH, D. A. ELLIOTT, K. KLAASEN, AND G. E. DANIELSON (1976a). Space–time relationships in the UV markings on Venus. *J. Atmos. Sci.* **33,** 1383–1393.

BELTON, M. J. S., G. R. SMITH, G. SCHUBERT AND A. D. DEL GENIO (1967b). Cloud patterns, waves and convection in the Venus atmosphere. *J. Atmos. Sci.* **33,** 1394–1417.

BLACKMAN, R. B., AND J. W. TUKEY (1958). *The Measurement of Power Spectra*. Dover, New York.

CHANG, C.-P. (1970). Westward propagating cloud patterns in the tropical Pacific as seen from time-composite satellite photographs. *J. Atmos. Sci.* **27,** 133–138.

COUNSELMAN, C. C., S. A. GOUREVITCH, R. W. KING, AND G. B. LORIOT (1980). Zonal and meridional circulation of the lower atmosphere of Venus determined by radio interferometry. *J. Geophys. Res.* **85,** 8026–8030.

COVEY, C., AND G. SCHUBERT (1981). Four-day waves in the Venus atmosphere. *Icarus* **47,** 130–138.

DOLLFUS, A. (1975). Venus: Evolution of the upper atmospheric clouds. *J. Atmos. Sci.* **32,** 1060–1070.

ESPOSITO, L. W. (1980). Ultraviolet contrasts and the absorbers near the Venus cloud tops. *J. Geophys. Res.* **85,** 8151–8157.

FELS, S. B., AND R. S. LINDZEN (1974). The interaction of thermally excited gravity waves with mean flows. *Geophys. Fluid Dyn.* **6,** 149–191.

GIERASCH, P. J. (1975). Meridional circulation and the maintenance of the Venus atmospheric rotation. *J. Atmos. Sci.* **32,** 1038–1044.

HANSEN, J. E., AND J. W. HOVENIER (1974). Interpretation of the polarization of Venus. *J. Atmos. Sci.* **31,** 1137–1160.

HANSEN, J. E., AND L. D. TRAVIS (1974). Light scattering in planetary atmospheres. *Space Sci. Rev.* **16,** 527–610.

KAWABATA, K., D. L. COFFEEN, J. E. HANSEN, W. A. LANE, M. SATO, AND L. D. TRAVIS (1980). Cloud and haze properties from Pioneer Venus polarimetry. *J. Geophys. Res.* **85,** 8129–8140.

KAWABATA, K., M. SATO, AND L. D. TRAVIS (1982). Polarimetric determination of aerosol properties and variation of haze and cloud structure on Venus. Submitted.

KUO, H.-L. (1949). Dynamic instability of two-dimensional nondivergent flow in a barotropic atmosphere. *J. Meteorol.* **6,** 105–122.

LANE, W. A., AND R. OPSTBAUM (1982). High altitude Venus haze from Pioneer Venus limb scans. Submitted.

LIMAYE, S. S., AND V. E. SUOMI (1981). Cloud motions on Venus: Global structure and organization. *J. Atmos. Sci.* **38,** 1220–1235.

MITCHELL, J. M. (1966). *Climatic Change.* WMO Technical Note No. 79, Geneva.

ROSSOW, W. B. (1978). Cloud microphysics: Analysis of the clouds of Earth, Venus, Mars, and Jupiter. *Icarus* **36,** 1–50.

ROSSOW, W. B., AND G. P. WILLIAMS (1979). Large-scale motion in the Venus stratosphere. *J. Atmos. Sci.* **36,** 377–389.

ROSSOW, W. B., A. D. DEL GENIO, S. S. LIMAYE, L. D. TRAVIS, AND P. H. STONE (1980). Cloud morphology and motions from Pioneer Venus images. *J. Geophys. Res.* **85,** 8107–8128.

RUSSELL, E., L. WATTS, S. PELLICORI, AND D. COFFEEN (1977). Orbiter cloud photopolarimeter for the Pioneer Venus mission. *Proc. Soc. Photo Opt. Instrum. Eng.* **112,** 28–44.

SATO, M., K. KAWABATA, AND J. E. HANSEN (1977). A fast invariant imbedding method for multiple scattering calculations and an application to equivalent widths of CO_2 lines on Venus. *Astrophys. J.* **216,** 947–962.

SCHUBERT, G., C. COVEY, A. DEL GENIO, L. S. ELSON, G. KEATING, A. SEIFF, R. E. YOUNG, J. APT, C. C. COUNSELMAN, A. J. KLIORE, S. S. LIMAYE, H. E. REVERCOMB, L. A. SROMOVSKY, V. E. SUOMI, F. TAYLOR, R. WOO, AND U. VON ZAHN (1980). Structure and circulation of the Venus atmosphere. *J. Geophys. Res.* **85,** 8007–8025.

SUOMI, V. E., AND S. S. LIMAYE (1978). Venus: Further evidence of vortex circulation. *Science* **201,** 1009–1011.

TAYLOR, F. W., R. BEER, M. T. CHAHINE, D. J. DINER, L. S. ELSON, R. D. HASKINS, D. J. MCCLEESE, J. V. MARTONCHIK, P. E. REICHLEY, S. P. BRADLEY, J. DELDERFIELD, J. T. SCHOFIELD, C. B. FARMER, L. FROIDEVAUX, J. LEUNG, M. T. COFFEY, AND J. C. GILLE (1980). Structure and meteorology of the middle atmosphere of Venus: Infrared remote sensing from the Pioneer Orbiter. *J. Geophys. Res.* **85,** 7963–8006.

THOMPSON, P. D. (1948). The propagation of permanent-type waves in horizontal flow. *J. Meteorol.* **5,** 166–168.

TRAVIS, L. D. (1978). Nature of the atmospheric dynamics on Venus from power spectrum analysis of Mariner 10 images. *J. Atmos. Sci.* **35,** 1584–1595.

TRAVIS, L. D. (1979). Imaging and polarimetry with the Pioneer Venus Orbiter cloud photopolarimeter. *Proc. Soc. Photo Opt. Instrum. Eng.* **183,** 299–304.

TRAVIS, L. D., D. L. COFFEEN, J. E. HANSEN, K. KAWABATA, A. A. LACIS, W. A. LANE, S. S. LIMAYE, AND P. H. STONE (1979a). Orbiter cloud photopolarimeter investigation. *Science* **203,** 781–785.

TRAVIS, L. D., D. L. COFFEEN, A. D. DEL GENIO, J. E. HANSEN, K. KAWABATA, A. A. LACIS, W. A. LANE, S. S. LIMAYE, W. B. ROSSOW, AND P. H. STONE (1979b). Cloud images from the Pioneer Venus orbiter. *Science* **205,** 74–76.

YOUNG, R. E., AND G. SCHUBERT (1973). Dynamical aspects of the Venus 4-day circulation. *Planet. Space Sci.* **21,** 1563–1580.

ZANGVIL, A. (1975). Temporal and spatial behavior of large-scale disturbances in tropical cloudiness deduced from satellite brightness data. *Mon. Weather Rev.* **103,** 904–920.